Predicting the stiffness and strength of human femurs with real metastatic tumors

Zohar Yosibash[a,*], Romina Plitman Mayo[a], Gal Dahan[a], Nir Trabelsi[b], Gail Amir[c], Charles Milgrom[d]

[a]*Department of Mechanical Engineering, Ben-Gurion University, Beer-Sheva, Israel*
[b]*Department of Mechanical Engineering, Shamoon College of Engineering, Beer-Sheva, Israel*
[c]*Department of Pathology, Hadassah University Hospital, Jerusalem, Israel*
[d]*Department of Orthopaedics, Hadassah University Hospital, Jerusalem, Israel*

Abstract

Background: Predicting patient specific risk of fracture in femurs with metastatic tumors and the need for surgical intervention are of major clinical importance. Recent patient-specific high-order finite element methods (p-FEMs) based on CT-scans demonstrated accurate results for healthy femurs, so that their application to metastatic affected femurs is considered herein.

Methods: Radiographs of fresh frozen proximal femurs specimens from donors that died of cancer were examined, and seven pairs with metastatic tumor identified. These were CT-scanned, instrumented by strain-gauges and loaded in stance position at three inclination angles. Finally the femurs were loaded until fracture that usually occurred at the neck. Histopathology was performed to determine whether metastatic tumors are present at fractured surfaces. Following each experiment p-FE models were created based on the CT-scans mimicking the mechanical experiments. The predicted displacements, strains and yield loads were compared to experimental observations.

Results: The predicted strains and displacements showed an excellent agreement with the experimental observations with a linear regression slope of 0.95 and a coefficient of regression $R^2 = 0.967$. A good correlation was obtained between the predicted yield load and the experimental observed yield, with a linear regression slope of 0.80 and a coefficient of

*Corresponding author
Email address: zohary@bgu.ac.il (Zohar Yosibash)

regression $R^2 = 0.78$.

Discussion: CT-based patient-specific p-FE models of femurs with real metastatic tumors were demonstrated to predict the mechanical response very well. A simplified yield criterion based on the computation of principal strains was also demonstrated to predict the yield force in most of the cases, especially for femurs that failed at small loads. In view of the limited capabilities to predict risk of fracture in femurs with metastatic tumors used nowadays, the p-FE methodology validated herein may be very valuable in making clinical decisions.

Keywords: Metastatic tumors, p-FEMs, femur

---

1. Introduction

One third to one half of all cancers (especially breast, prostate, renal, thyroid, and lung cancer) metastasize to bones [3], which in turn leads to pathologic fractures or symptoms severe enough to require treatment in 30-50% of these cases [9]. Currently, to assess the fracture risk in patient with skeletal metastasis clinicians use the Mirels' criterion or rely on their past clinical experience. The Mirels' criterion is however not very specific (91% sensitive, 35% specific) [18, 4] and results in unnecessary internal fixation procedures in two thirds of the patients.

In recent years more accurate methods based on computed tomography (CT) have been suggested to predict the risk of fracture that take into consideration both the patient specific geometrical description and the spatial distribution of material properties in bones with metastases (especially lytic types). These include the CT based structural rigidly analysis (CTRA) that is mainly applicable to shaft regions [21, 19] and CT based finite element methods (FEMs) [13, 14, 22, 15, 23, 5]. A summary of past FE investigations for human femurs with realistic/simulated metastatic tumors is given in Table 1.

Most past studies that use FEMs for the assessment of fractures risk in femurs with metastases are limited because they are "validated" by healthy bones with artificially created defects that do not well represent actual metastatic tumors.

Metastases are associated with major trabecular bone loss before cortical bone loss and

Reference	# of femurs	Kind of test
Keyak et al. [13]	12 shafts (death=cancer)	4PB
Keyak at al. [14]	44 femurs (8 with metastases)	Compression
Spruijt et al. [22]	22 healthy shafts	Torsion
Tanck et al. [23]	12 healthy femurs	Compression
Deriks et al. [5]	20 healthy pairs	Compression

Reference	Defects description	Comments
Keyak et al. [13]	Realistic	FE+Exp on femur shafts
Keyak at al. [14]	Realistic	FE+Exp on proximal femurs
Spruijt et al. [22]	Transcortical hole subtrochanteric region	FE+Exp on shafts
Tanck et al. [23]	Drilled	FE+Exp on proximal femurs
Deriks et al. [5]	Drilled	FE+Exp on proximal femurs

Table 1: Summary of past FE simulations validated by experiments on human femurs with realistic/simulated tumors.

a considerable percentage of these tumors are mixed blastic-lytic ones. In addition, the borders between tumor and non-tumor affected areas usually do not have sharp boundaries. In this respect we cite [13], *"...we found that femoral shafts with hemispheric burr holes do not accurately simulate the force versus displacement behavior of shafts with metastatic lesions."* To the best of the authors' knowledge, the only previous study that considers FEMs of fresh frozen proximal femurs with real metastases that are validated by experimental observations is [14]. In that pioneering study eight femurs with metastatic tumors, out of 44 femurs altogether, are considered for the determination of the fracture load. In [14] the authors had to artificially alter the material properties of the bone tissue in the FE analysis on a "calibration cohort" of 18 femurs, 4 of which are with metastases (by comparing FEM fracture loads to the ones in experiments) to enable a better prediction of subsequent 26 femurs (4 with a metastasis). In spite of the fact that fracture occurrence is based on stress and/or strain criteria, none of the previous publications on the topic report on any validation

procedure for these quantities. Finally, none of these past publications performed histological analyses of the fractured bones to determine the type of metastases and whether the presence of a tumor influenced the fracture location.

Leveraging the success of predicting the mechanical response of intact femurs with very high accuracy by high-order FEMs [27, 31, 25, 26], we extend the developed methods to femurs with metastatic tumors. There are four novelties in the present study: a) A large cohort of femurs with realistic metastatic tumors (fourteen femurs from seven donors) is considered; b) A variety of metastatic tumors representing several different types of cancers are investigated; c) A detailed and thorough investigation of the femur's mechanical response (displacements and strains are validated); d) Pathological examination of the fracture surface to identify whether metastases are present and the precise tumor type.

We aim to provide rigorous evidence that patient-specific high-order FEMs are accurate and reliable to be used as a decision support system by orthopedic surgeons, especially in complex situations of femurs with metastatic tumors.

2. Materials and Methods

Fourteen fresh-frozen human femurs (7 pairs denoted by FFM1-FFM7) with proximal metastatic tumors were chosen by an experienced orthopedic physician based on radiographs (see Figure 1) and cause of death. Donor details are summarized in Table 2. These femurs underwent mechanical experiments after they were defrosted, cleaned of soft tissues and degreased with ethanol. The proximal femur ($\sim$ 250 mm from the top of the head) was fixed into a cylindrical metallic sleeve by PMMA, immersed in water and CT-scanned with K_2HPO_4 calibration phantoms. A Phillips Brilliance 64 CT axial scan without overlap (Einhoven, Netherlands - 120-140 kVp, 250 mAs, 0.75 - 1.5 mm slice thickness) was used with pixel size of 0.2-0.7 mm. Thirteen uniaxial strain gauges (SGs) (Vishay CEA-06-062UR-350) were bonded to the surface of each femur at the typical locations shown in Figure 2. Details on the procedure are available in [31].

Donor Label	Age (Years)	Height [m]	Weight [Kg]	Gender	Cause of Death
FFM1	77	1.80	50	Male	Lung Cancer
FFM2	74	1.50	45	Female	Colon Cancer
FFM3	55	1.75	73	Male	Pancreatic Cancer
FFM4	79	1.62	55	Female	Breast Cancer
FFM5	76	1.60	50	Female	Renal Cell Cancer
FFM6	71	1.90	84	Male	Prostate Cancer
FFM7	75	1.62	41	Female	Cervical Cancer

Table 2: Donor details.

2.1. In-vitro experiments

Mechanical experiments were conducted on each pair (right and left femurs) on the day of defrosting in a configuration that mimics a simple stance position (see Figure 3). The femurs were loaded through their head by a flat plate (on a 1-cm diameter circular surface) and clamped at the distal part. Loading was applied at three different inclination angles (0°, 7° and 15°), see Figure 3. Most of the experiments were performed with a Shimadzu AG-IC machine (Shimadzu Corporation, Kyoto Japan) having a load cell of 20kN (precision of $\pm 0.5\%$). Strains, forces and vertical and horizontal displacements of the head (U_z and U_x) were recorded by a Vishay 7000 data-logger. To confirm repeatability, each loading was repeated two to six times at a rate of 5 $\frac{mm}{min}$. The linear elastic response was checked for each SG at each loading and inclination by a linear regressions analysis. Experimental results beyond 150 N (pre-load) were analyzed: the average slope ($\Delta strain/\Delta F$) of each SG was calculated and normalized to 1000 N for comparison with the FE results. The same procedure was followed for the displacements.

After the completion of the mechanical experiments each femur was loaded in the 15° configuration at a rate of 1000 $\frac{mm}{min}$ to fracture. The force, displacements and strains were recorded to monitor the instance of "yielding", i.e. when the mechanical response deviates from linearity. Yielding is based on the three SGs closest to the fracture, and is defined as

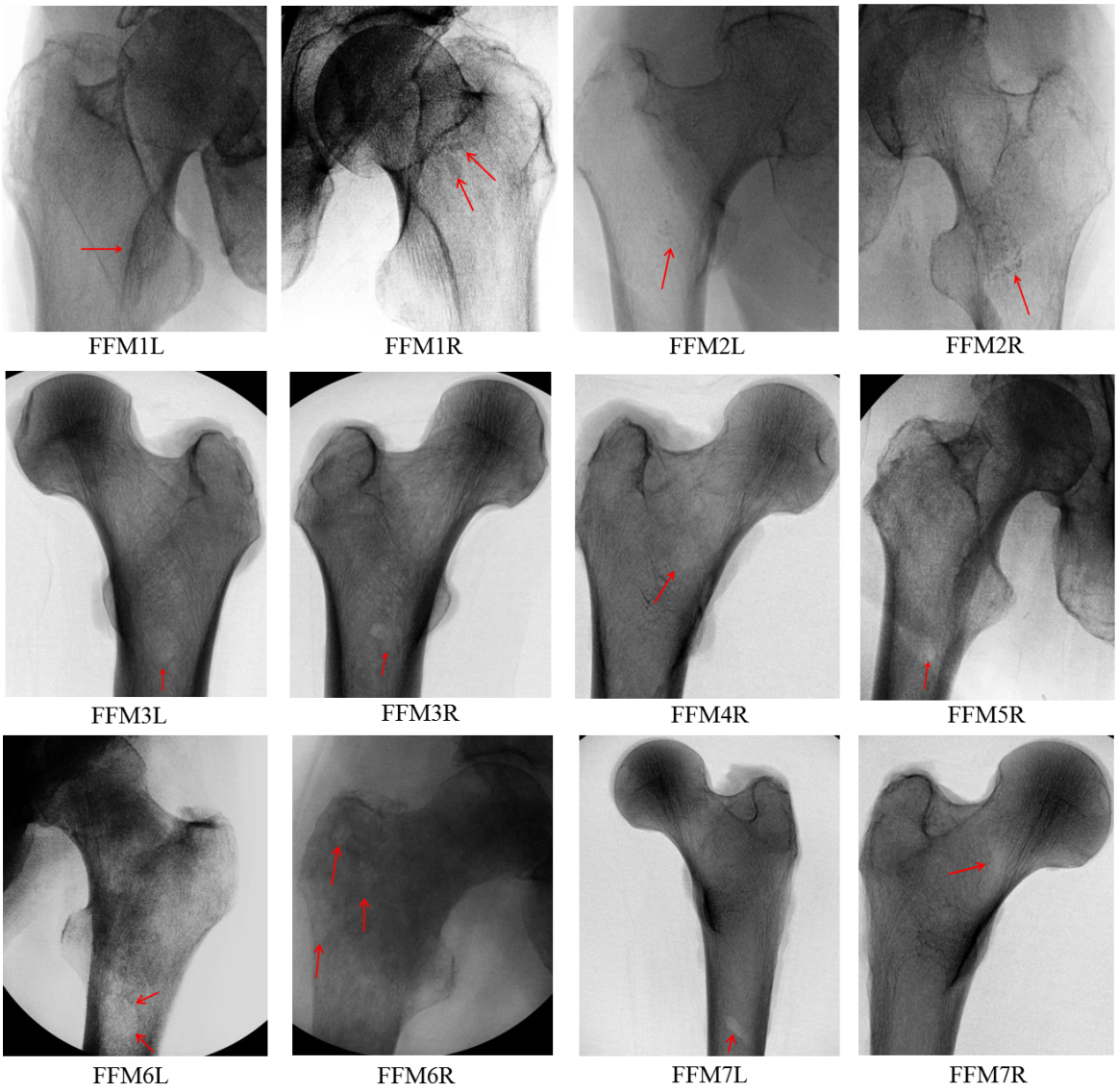

Figure 1: Radiograph images of femurs with suspected tumors (pointed to by arrows).

the force at which a 5% slope deviation in the linear force-strain slope is noticed in the first SG. The lower limit for yielding is defined at the instance of departure of the force-strain curve from linearity (see Figure 4). The ultimate force was defined as the force at fracture (highest force recorded). The fracture initiation location is determined from videos taken during the experiments but the exact location can not always be detectable.

After fracture the proximal femurs were refrozen until histopathology examination at

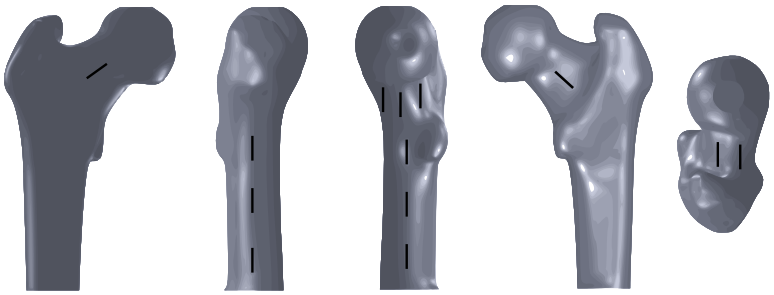

Figure 2: Typical SGs locations.

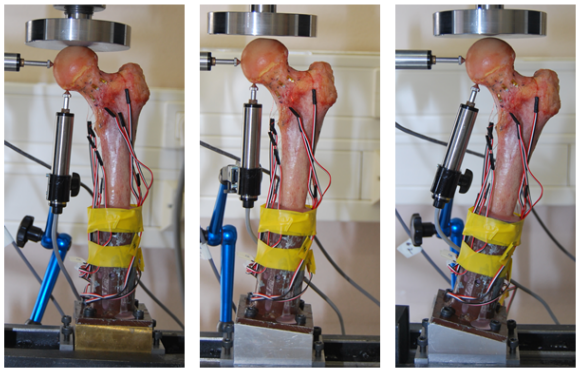

Figure 3: Typical experiments at three inclination angles.

which time they were sequentially thawed, fixed, decalcified, embedded and sectioned. Histological examination was done by a bone pathologist.

2.2. FE analyses

Finite element analyses mimicking the experimental procedure were performed to determine whether they can predict the mechanical response and the instance of fracture initiation compared to the experimental observations. The QCT-based high-order FE models were semi-automatically constructed following the methods detailed in [27, 31]. Pixel sizes for the scanned femurs are summarized in Table 3.

The FE femur models were verified and validated by experimental observations on fresh frozen *healthy* femurs, see e.g. [26]. The FE model construction is briefly described herein. All DICoM (Digital Imaging and Communication in Medicine) format QCT scans were *au-*

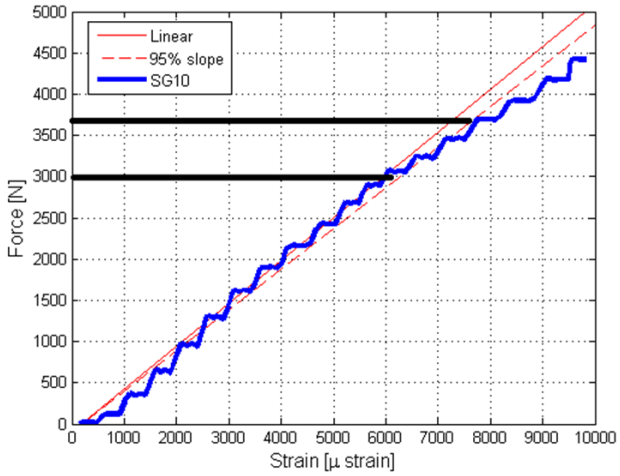

Figure 4: Typical graph for determining yield load.

Femur Label	FFM1R	FFM2R	FFM3R	FFM4R	FFM5R	FFM6R	FFM7R
Pixel Size (mm)	0.2373	0.2392	0.1953	0.1953	0.2461	0.2314	0.1953
Femur Label	FFM1L	FFM2L	FFM3L	FFM4L	FFM5L	FFM6L	FFM7L
Pixel Size (mm)	0.2119	0.2441	0.1953	0.1953	0.2353	0.2561	0.2617

Table 3: CT pixel size for each femur.

tomatically manipulated by in-house Matlab programs. The proximal femur bone's axis was aligned with the z axis. Since no exact Hounsfield Units (HU) exist that distinguish between the cortical and trabecular bone we associated values of HU$>$ 475 ($\rho_{ash} > 0.486\ g/cm^3$) with the cortical bone and values of HU$\leq$ 475 to trabecular bone according to [1, 6, 8, 2]. CT data was manipulated by a 3-D smoothing algorithm that generates clouds of points each representing the femur's exterior, interface and interior boundaries. These clouds of points were imported into the CAD package SolidWorks[1] that generated a surface representation of the femur and subsequently a solid model. The resulting 3D solid was imported into a high-order FE code where a tetrahedral FE mesh was created and mesh refined at areas of interest. The entire algorithm (QCT to FE model) is schematically illustrated in Figure 5.

[1]A CAD (computer-aided design) program developed by Dassault Systems SolidWorks Corp.

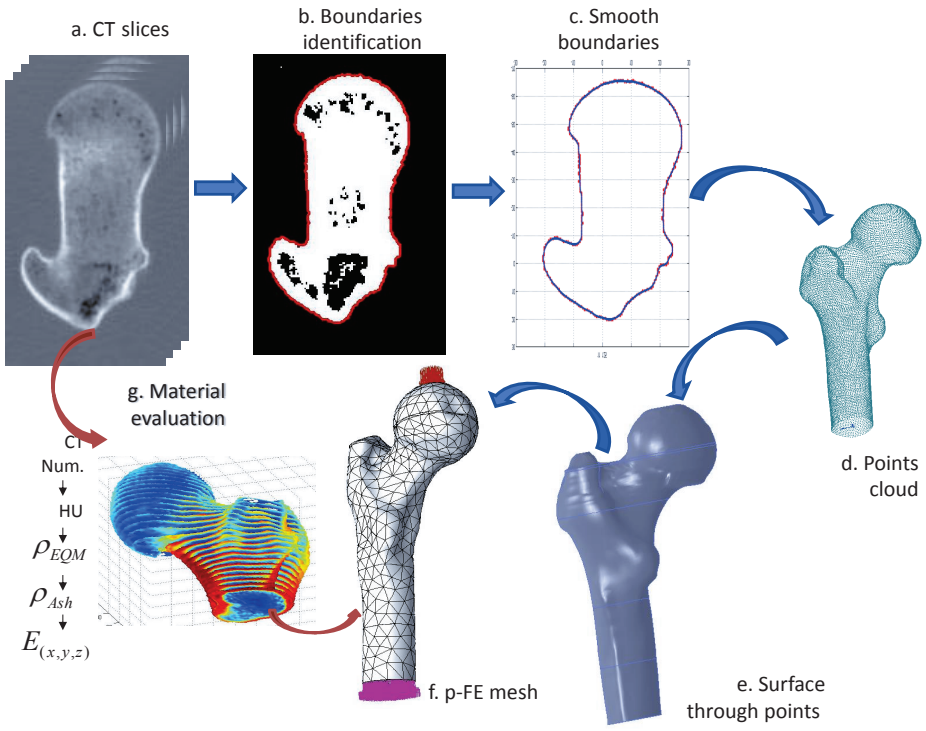

Figure 5: Schematic flowchart describing the generation of the p-FE model from QCT scans. a - Typical CT-slice, b. - Contour identification, c. - Smoothing boundary points, d. - Points cloud representing the bone surface, e. - Bone surface, f. - p-FE mesh and g. - Material evaluation from CT data.

High-order FEMs (p-FEMs) were chosen because of their many advantages over their classical FEMs counterparts: numerical convergence is considerably faster, p-FEMs allow functional variation of the material properties within each element, the FEs may be large and be by far more distorted and yet produce considerable faster convergence rates. In addition, p-FEMs accurately represent the bone's smooth surfaces.

2.2.1. Assignment of material properties to FE models

Inhomogeneous isotropic material properties were assigned to the FE model at 512 Gauss points within each tetrahedral element. Although anisotropic material properties are known to better represent the bone tissue (see [24, 16] and references therein), for the stance position loading isotropic approximation has shown to approximate femur's mechanical response well.

Most of the suspected tumors were not visualized in the CT images or did not have a

well defined boundary. Therefore, the tumors were assigned the same material properties (according to their mineral bone density) as any other bone tissue in the FE model. This methodology has already been identified as appropriate in [14]: *"It is important that these relationships be applicable to bone with and without metastases because it is difficult to reliably identify specific areas of metastatic involvement in a bone. Therefore, instead of applying different mechanical property relationships to areas with and without metastatic involvement, the relationships presented here can be applied universally throughout. The levels of precision and accuracy achieved in this study indicate that this methodology was successful and shows the robustness of this modeling method."*

K_2HPO_4 liquid phantoms [17] were placed near each femur while immersed in water during the CT scan. These phantoms were used to correlate the known mineral density and HUs:

$$\rho_{K_2HPO_4}\ [gr/cm^3] = 10^{-3} \times (0.8072 \times HU - 1.6) \tag{1}$$

The ash density ρ_{ash} is determined based on recent empirical connections [20], using the connection between hydroxyapetite and K_2HPO_4 phantoms [7]:

$$\rho_{ash}\ [gr/cm^3] = 0.877 \times 1.21 \times \rho_{K_2HPO_4} + 0.08 \tag{2}$$

The relation reported in [11] includes specimens with a wide density range ($0.092 < \rho_{ash} < 1.22\ [g/cm^3]$) while the relation reported in [12] was obtained using ash densities $< 0.3\ [g/cm^3]$. The ρ_{ash} threshold between cortical and trabecular tissues is unclear, however all the pixels having HU number larger than 475 are considered cortical bone. HU=475 leads to $\rho_{ash} = 0.486$ using (1) and (2) based on previous publications [29, 31, 10]. Thus, the following relations were used to determine Young's modulus from ρ_{ash}:

$$E_{cort} = 10200 \times \rho_{ash}^{2.01}\ [MPa], \quad \rho_{ash} \geq 0.486 \tag{3}$$

$$E_{trab} = 2398\ [MPa], \quad 0.3 < \rho_{ash} < 0.486 \tag{4}$$

$$E_{trab} = 33900 \times \rho_{ash}^{2.2}\ [MPa], \quad \rho_{ash} \leq 0.3 \tag{5}$$

Young's modulus at the transition area between cortical and trabecular bone tissue ($0.3 < \rho_{ash} < 0.486$) was set to $E = 2398$ $[MPa]$, based on the data reported in the literature. Poisson ratio was set to $\nu = 0.3$.

2.2.2. Boundary conditions and post-processing of FE results

To mimic the experimental setup, a compression force of 1000 N was applied on a planar circular area (10mm diameter) at the superior surface of the femoral head (see Figure 6) at the respective angles (0°, 7° and 15°). The FE models for all specimens were fully constrained at the distal part of the shaft. Since femurs undergo linear mechanical response under small strains, only linear analyses were performed. The creation of each model took approximately two hours and their solution about eight hours on average.

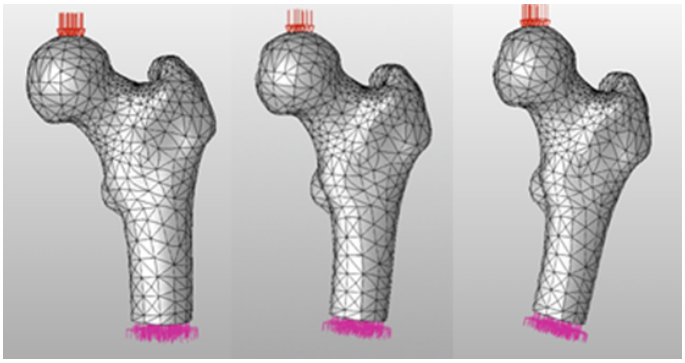

Figure 6: Boundary conditions on the FE models (a)0° (b) 7° (c) 15°.

The p-FE models were solved by increasing the polynomial degree until convergence in energy norm was observed (all models had an error in energy norm of $< 10\%$). Thereafter, verification of convergence was performed to all strains and displacement at the regions of interest. In case of poor local convergence, a local refinement and a new analysis was performed.

The average strain along element edges was extracted from FE results since it best represents the average strain surface recorded by the SGs. Displacements were extracted at nodes. Because uni-axial SGs were used in all experiments, the FE strain component was considered in the direction coinciding with the SG direction, which usually were aligned along the local

principal strain directions (E_1 or E_3). If the SG was found not to align with the principal strain, a local axis system was positioned and the value was extracted relatively to the new system.

The predictability of the finite element analyses was examined by comparing the FEA results with the experimental observations. Statistical analysis is based on a standard linear regression, where a perfect correlation is evident by a unit slope, a zero intercept and a unit R^2 (linear correlation coefficient). The results are shown also in a Bland-Altman error plot $((EXP - FE),\ \frac{EXP-FE}{2})$. The mean error and the absolute mean error values were also calculated:

$$\text{Mean Error} = \frac{100}{N}\ \Sigma_{i=1}^{N}(Exp_{(i)} - FE_{(i)})/Exp_{(i)} \quad [\%] \tag{6}$$

$$\text{Mean absolute Error} = \frac{100}{N}\ \Sigma_{i=1}^{N}\left|(Exp_{(i)} - FE_{(i)})/Exp_{(i)}\right| \quad [\%] \tag{7}$$

Predicting yield force: A simplified yield strain criterion, previously shown to predict the yield of healthy fresh frozen femurs reasonably well in [29], was used herein to estimate the yield of the cancer affected femurs. This criterion estimates the yield initiation to occur at the location where the largest principal strain (by a linear elastic analysis) on bone's surface reaches a critical value of 7300 μstrains in tension or -10400 μstrains in compression (reported in [2]). The principal strains on femur's surface were computed for an applied 1000 N. The ratio between the critical strain in tension (respectively compression) to the maximum (respectively minimum) computed principal strain times 1000 N was determined as the predicted yield force. Because pointwise values of FE strains may contain large numerical errors, we used instead an averaged value along a part of an element edge adjacent to the maximum strain location.

3. Results

3.1. Experimental results

Strains and displacements recorded during the mechanical tests showed a linear relationship with the applied load (excluding the fracture experiments) as shown by a typical example

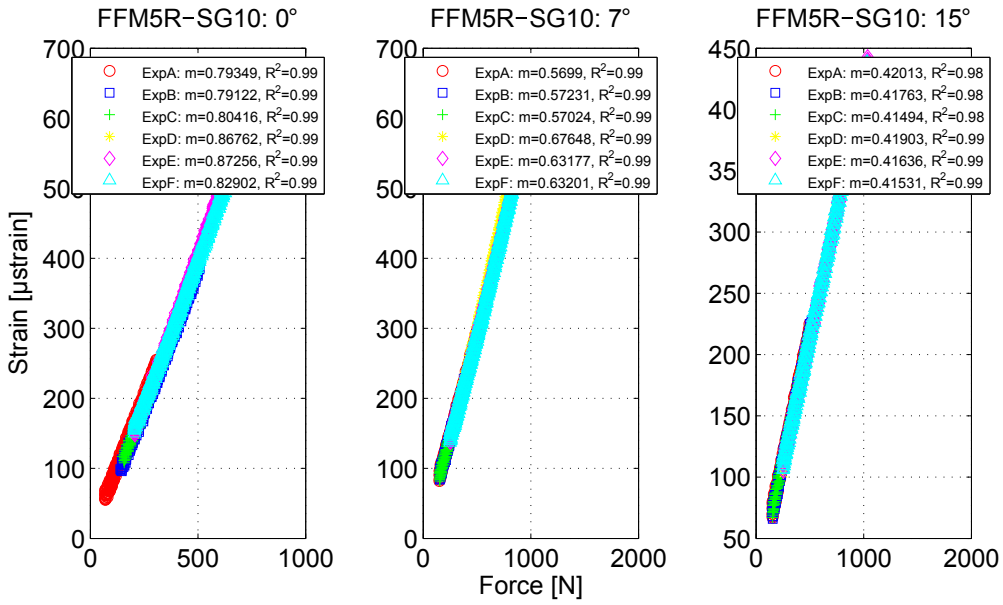

Figure 7: Typical strain gauge response for the three angles (FFM5R-SG10).

in Figure 7. A non-typical response was noticed for the FFM2 pair, i.e. an increase in strains with an increase in the femoral inclination angle. This response was not previously noted in any of our prior experiments on 31 femoral specimens. Therefore the FFM2 results were excluded with the belief that they represented an experimental error.

Following the elastic experiments, all fourteen femurs were loaded to failure at an inclined angle of 15 degrees while their response was monitored (one femur, FFM4L was accidentally fractured at 7°). Except for the two femurs FFM1R and FFM1L that did not break after applying 12,000 N, all other femurs broke at much lower loads. On FFM1R and FFM1L the applied displacement on femurs head was maintained for 8-13 seconds during which the femurs broke suddenly showing a creep-like phenomenon. Details are provided in [28]. A summary of the fracture experiments is given in Table 4. Most of the femurs showed a small plastic deformation before fracturing (yield loads were smaller than fracture loads).

Figure 8 presents the fracture patterns in the femurs. Figure 9 presents the applied force vis. measured strain at the SG closest to the failure location and head's displacement until fracture.

Figure 8: Fracture patterns in femurs.

All fractured surfaces underwent histopathology examination and in 8 of the 14 femurs metastatic tumors were found (Figure 10).

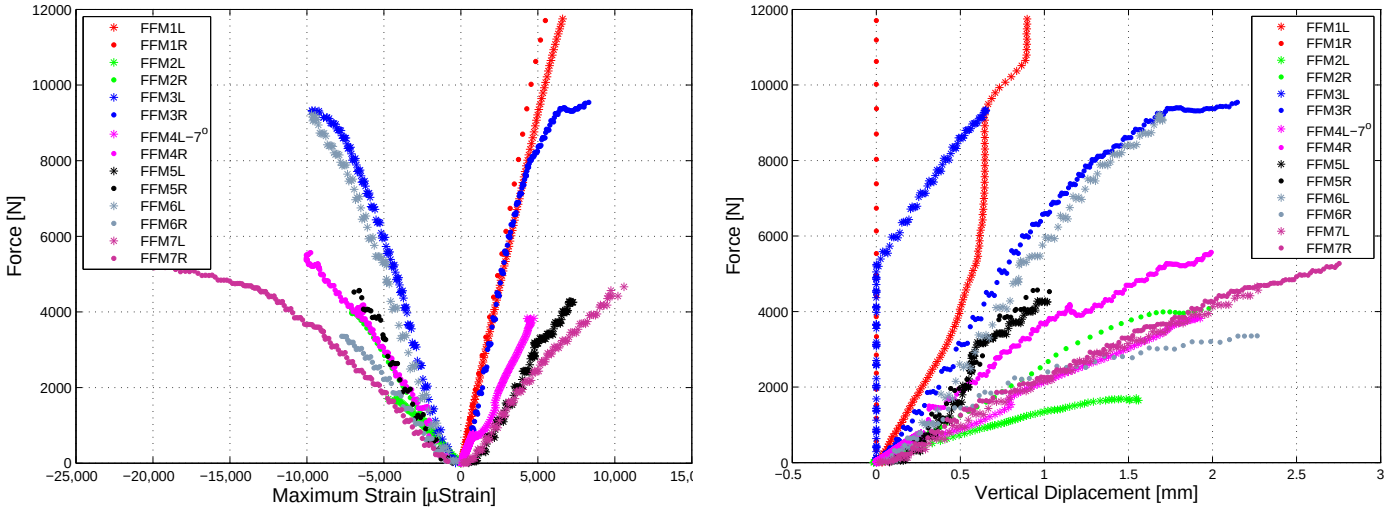

Figure 9: Fracture experiment (a) strains and (b) vertical head displacement measurements for all femurs.

Femur #	Deviation from linearity [N]	Deviation from 5% linearity [N]	Ultimate Force [N]	Fracture Type	Location of fracture initiation	Tumor on fracture surface
FFM1R	11800	11800	>12000	T	UNHJ	Lytic Adenocarcinoma near fracture surface
FFM1L	10300	11500	>12000	T	Upper middle neck	Lytic Adenocarcinoma
FFM2R	3650	3950	4000	U	Upper middle head	None
FFM2L	1650	1650	1700	T	UNHJ	None
FFM3R	7500	8200	10150	T	UN	None
FFM3L	8600	9000	9700	T	UN	None
FFM4R	5600	5600	5600	T	UN	Lytic Breast Cancer
FFM4L	3650	3650	3800	T	UNHJ (7°)	Lytic Breast Cancer
FFM5R	3800	4200	4550	T	UNHJ	Lytic Renal Cell Cancer
FFM5L	3400	4200	4500	T	UNHJ	Lytic Renal Cell Cancer
FFM6R	3200	3200	3400	T	Proximal part,under greater trochanter	Blastic Prostate Cancer
FFM6L	7800	8400	9100	U	Upper middle head	Blastic Prostate Cancer
FFM7R	4100	4600	5300	U	UN	None
FFM7L	3000	3700	4670	T	UNHJ	None

T = Tension, U = Unknown, UN = Upper neck, UNHJ = Upper neck-head junction.

Table 4: Fracture experiments summary.

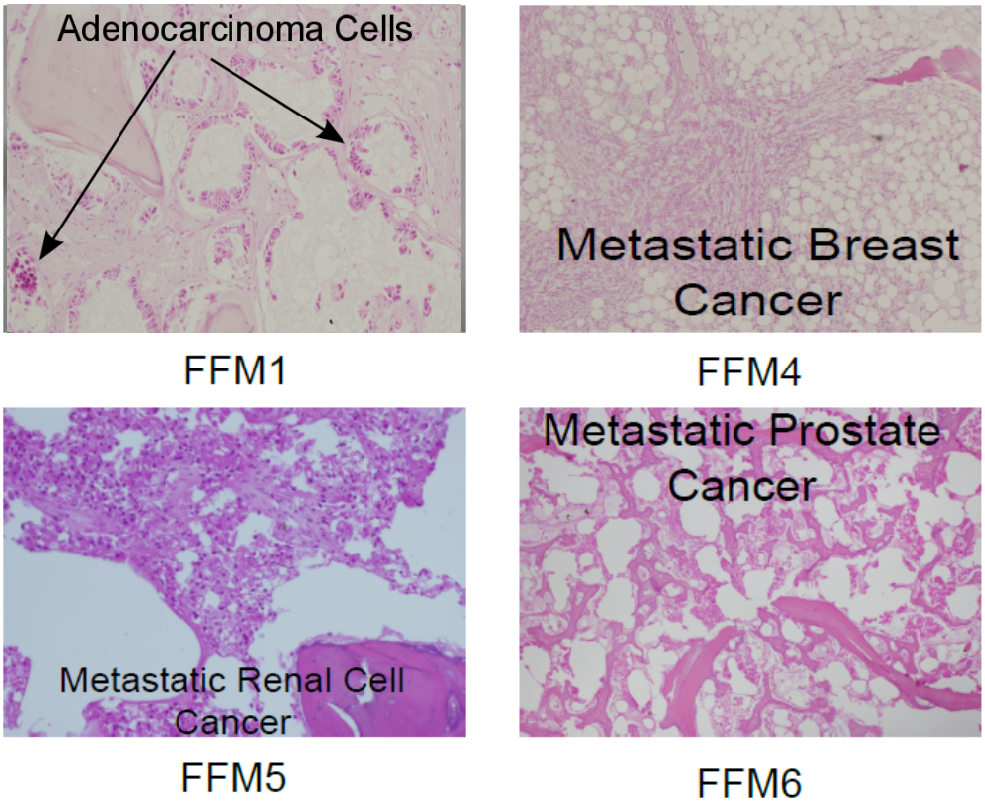

Figure 10: FFM1 = Metastases in both bones. FFM1R near fracture surface, FFM1L on fracture surface. FFM4 = Metastases on fracture surfaces. FFM5 = Metastases on fracture surfaces. FFM6 = Metastases on fracture surface. FFM2 = No metastases extreme osteoporosis. FFM3, FFM7 = No metastases.

3.2. Mechanical response: FE results compared to experimental observations

The principal strain E_3 at 1000 N computed for the fourteen femurs at 0^o is shown in Figure 11.

The relative error in energy norm converged to less than 10% at $p = 8$ for all load cases in all femurs, and the displacements and strains at the points of interest converged within 1% error between $p = 7$ and $p = 8$. The correspondence between the FE results and experimental observations for each femur excluding FFM2 is summarized in Table 5, including the statistical measures. A linear regression and Bland-Altman error plots that compare the FE and experimental results(64 displacement measurements and 420 strain measurements), are shown in Figure 12 and 13.

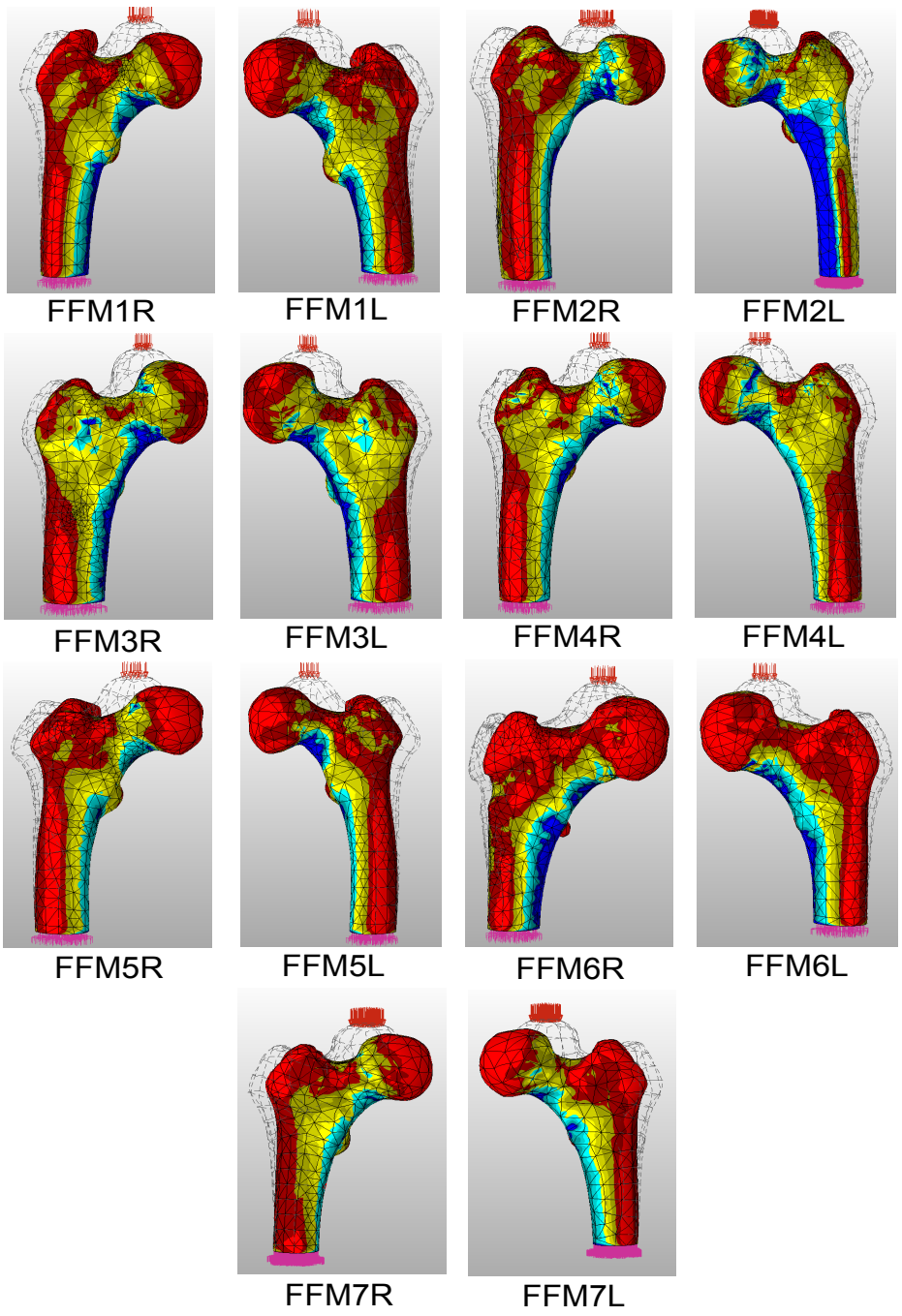

Figure 11: Principal strain E_3 at 1000 N load computed by p-FE analyses for the fourteen femurs at 0^o inclination (colors not at same scales for all models).

Bone (label)	Linear Correlation	R^2	Mean error (%)	Mean absolute error (%)
FFM1R	FE= 1.059 × EXP+2.96	0.982	-4	14
FFM1L	FE=0.956 × EXP-9.30	0.976	-2	13
FFM3R	FE=0.935 × EXP-2.79	0.951	0	14
FFM3L	FE=1.016 × EXP-0.68	0.981	-5	14
FFM4R	FE=0.917 × EXP+33.05	0.981	-1	15
FFM4L	FE=1.038 × EXP+34.86	0.980	-12	15
FFM5R	FE=0.997 × EXP+16.35	0.992	-2	14
FFM5L	FE=0.926 × EXP-19.74	0.990	-9	8
FFM6R	FE=0.838 × EXP-51.53	0.952	9	19
FFM6L	FE=0.960 × EXP-0.70	0.982	-2	12
FFM7R	FE=1.096 × EXP-153.0	0.946	-13	23
FFM7L	FE=0.950 × EXP-103.3	0.980	13	16
All	**FE=0.949 × EXP-25**	**0.957**	**-0.8**	**14.8**

Table 5: Summary of statistical measures for the biomechanical response of the individual femurs.

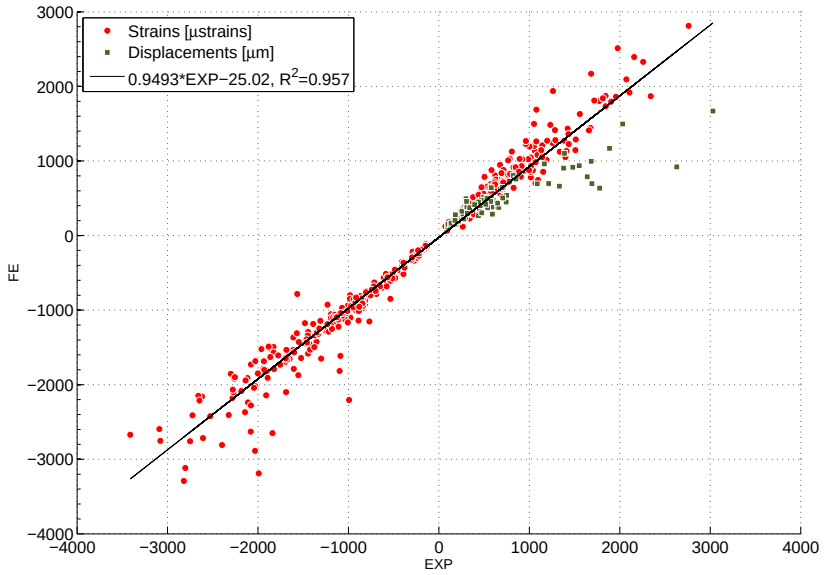

Figure 12: Linear correlation for all biomechanical data excluding FFM2 (strains and displacements on femurs' boundaries).

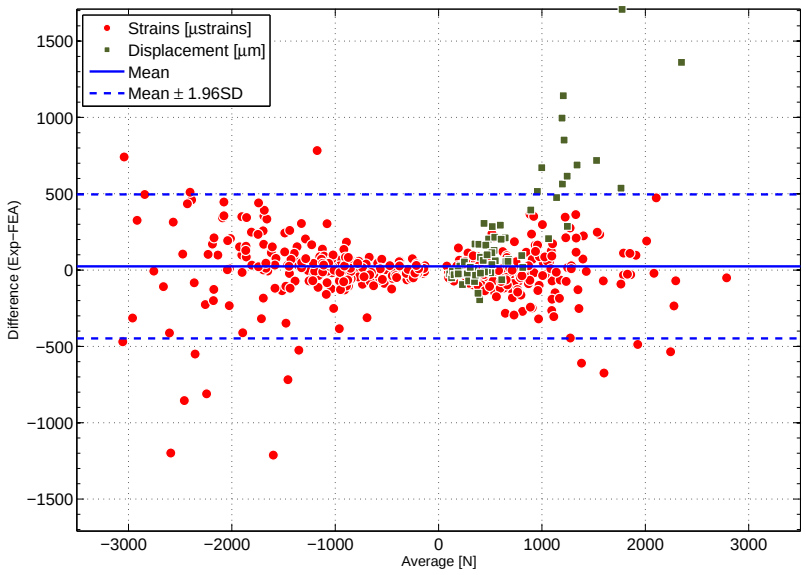

Figure 13: Bland-Altman error plot for all biomechanical data excluding FFM2 (strains and displacements on femurs' boundaries).

3.3. Prediction of fracture load and location

Table 6 summarizes the yield load predicted by the FE analysis as compared to the estimated yield load and the ultimate load in the experiment. The correspondence between the yield location predicted by the FE analysis and the fracture location in the experiment is also marked: ✔ denote a FE analysis that predicts yield at the same location as fracture initiation is observed in experiment, ✖ denotes a disagreement between the FE predicted yield and fracture locations and ✯ denotes a fracture of the head beneath the loading plate that was not modeled properly in the FE analysis.

FFM	1R	1L	2R	2L	3R	3L	4R	4L	5R	5L	6R	6L	7R	7L
5% EXP	11800	11500	3950	1650	8200	9000	5600	3650	4200	4200	3200	8400	4800	3700
FE	5620	5510	3100	1250	6600	5600	4110	2920	4700	2810	3650	7400	3730	3800
Exp Ult	>12000	>12000	4000	1700	10150	9700	5550	3800	4550	4500	3400	9100	5300	4700
Location	✖	✔	✯	✔	✔	✔	✖	✔	✔	✖	✔	✯	✖	✔

Table 6: Yield load in experiments, estimated by the FE analysis and the ultimate load in experiments ([N]).

Figures 14 and 15 show the linear regression of the yield load predicted by the FEA and estimated in the experiments, and the associated Bland-Altman graph. In these graphs the FFM1 femurs are excluded because they fractured at a very high load in a creep-like mode.

4. Discussion

When presented with a patient with a metastatic long bone tumor the physician must make several clinical decisions. These are dependent on the projected treatment response of the lesion, the mechanical strength of the affected bone and the patient's estimated life expectancy. If the tumor is deemed possibly responsive to treatment, then its strength may be expected either not to deteriorate or even to increase. On this basis the physician must decide either to allow the patient normal activities, advise protected ambulation, or to strengthen the bone with a surgical implant. Reliable patient specific criteria for determining the bone strength of a bone with a metastatic lesion are not currently available to the physician. The current study was designed to see if a patient specific tool with these abilities could be developed.

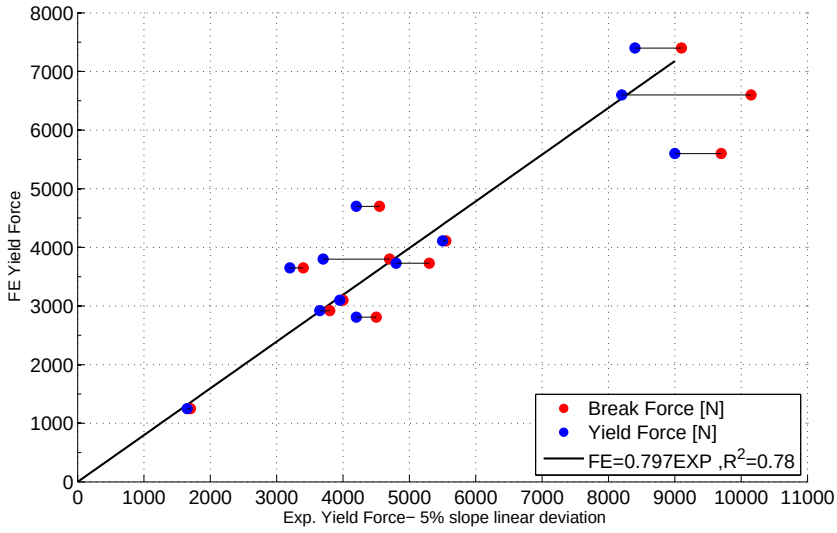

Figure 14: Linear correlation for yield load excluding FFM1.

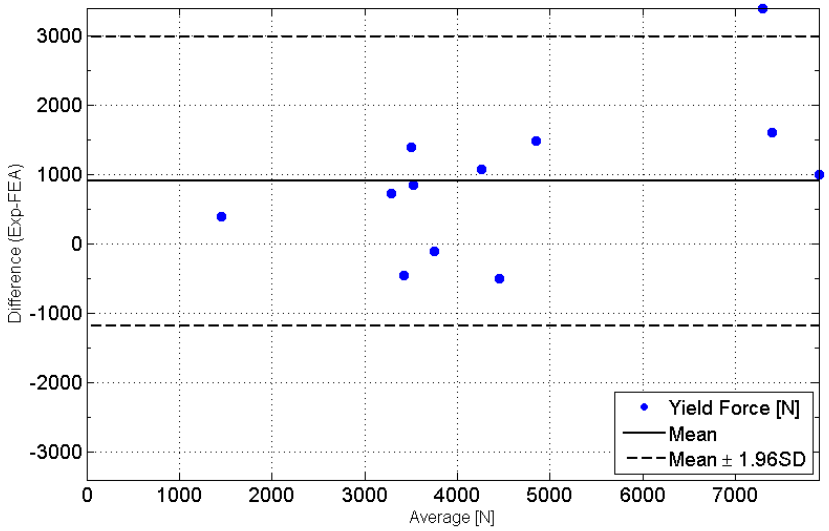

Figure 15: Bland-Altman error plot for yield load excluding FFM1.

The use of patient specific CT-based p-FEA to predict the biomechanical response of healthy femurs has been demonstrated to provide excellent results [30, 26]. Leveraging on this capability, a natural question was raised whether CT-based p-FEA may be applied with

the same success to femurs with metastatic tumors. To the best of our knowledge, this is the first work that investigates the mechanical response of femurs with actual metastatic tumors.

Femurs with metastatic tumors are of major concern due to the risk of *spontaneous* pathological fractures, that may occur during activities of daily living. For this reason, we considered loads that were applied to the femoral head that mimic stance position. We performed mechanical experiments and FE analyses on a large cohort of fourteen femurs suspected to contain metastatic tumors. This is the largest cohort of such femurs among previous publications on the topic: in [23, 5] ten femurs (healthy with holes that mimic metastatic tumors) were considered, and in [13] twelve femurs with metastatic tumors were considered.

The predicted strains and displacements showed an excellent agreement with the experimental observations with a linear regression slope of 0.95 and a coefficient of regression R^2 = 0.967. In the analysis of the mechanical response the pair of femurs FFM2 was excluded because of an unusual experimental response that can be attributed to experimental errors. Altogether 420 strains and 64 displacements from twelve femurs were analyzed.

Since most of the suspected tumors were not recognized in the CT images or did not have a well defined boundary, the same density-material properties relations as any other bone tissue was assigned to them in the FE model (as in [14]). These results suggest that there is no need for a special tumor E-ρ_{ash} relationship since the effect of metastases is accounted for due to density changes. Even though most of the tumors were not visible in the CT scans, the FE models provided good results. This implies that CT based p-FEMs are capable of predicting the mechanical response of femurs without knowledge of tumor's presence or tumor specifically representation. The wide diversity of tumor (blastic, lytic and mixed) and cancer types involved in this work contributed to the reliability of the proposed methodology.

The results also emphasized that drilling holes in healthy femurs to mimic metastatic tumors, as reported in several past publications, may not well represent actual metastatic tumors in bones.

Our FE predictions were considerably better for strains than for displacements. This is because we clamped the distal part of the femur in the FE analysis so that the FE dis-

placements were smaller compared to the ones measured in the experiment where the bone's distal part was embedded into PMMA and had some elastic displacement (this observation was confirmed by other FEA and experiments lately performed by the authors). The Bland-Altman plot in Figure 13 shows that the mean is unbiased, and 95% of the computed strains are within $\pm 500\mu$strain of the measured ones within the range $\pm 3000\mu$strains. The mean (6) and absolute mean (7) errors for the overall results (excluding FFM2) are -1% and 14.8%, respectively. The differences between the predicted and measured strains and displacements are considered low compared with past studies, especially for the fresh frozen femurs in this work that were affected by malignant tumors. In general, the FE predictions provided slightly smaller values than the measured ones, implying that the femur FE models are slightly stiffer compared to the actual femurs, possibly because of the weakened femurs due to the metastatic tumors.

Regarding the prediction of the risk of bone yielding (a non-reversible damage accumulated in the bone tissue), all past publications that use FEA for the determination of fracture onset in femurs with metastases based their predictions on some sort of stress-criterion. However, the use of FE stresses necessitates first ensuring that the computed stresses are accurate and correlated to in-vitro experiments before being used to determine any fracture instance. To the best of our understanding, past FE stresses were not compared to any experimental observations to demonstrate their validity. Furthermore, there is no evidence that stress-based fracture criterion (usually the von-Mises yield criterion) are appropriate for bone tissue.

In this research, we used a simplified yield strain criterion [29] to estimate the yield of the cancer affected femurs. Excluding the pair of femurs FFM1R and FFM1L, that fractured under a creep phenomenon after applying over 12000 N, we demonstrated a good correlation between the predicted yield load and the experimental observed yield, with a linear regression slope of 0.80 and a coefficient of regression $R^2 = 0.78$. In almost all cases the predicted yield load was lower compared to the experiment, demonstrating the conservative prediction (i.e. should the criterion be used in clinical practice, the yield is predicted before the femur yields).

Notice that yield load almost coincides with the ultimate load for femurs that fractured

at relatively low loads, and that the FE predictions for these cases are relatively accurate. This is of great clinical importance because only for these femurs is it important to accurately predict the risk of yielding, whereas there is no biomechanical concern for femurs that have large predicted yield loads.

In eight of the fourteen femurs the fracture surface passed through the metastatic tumor or very close to it. The metastatic tumor in seven out of the eight femurs was confined to the cancellous portion of the femur and not in the cortex. Pathology results showed that metastases to the bone have a significant influence on the fracture location, no matter what type of tumors (lytic or blastic) or type of cancer is present. The only femur that had a clearly demonstrated large tumor in the cortex (FFM6R), was clearly identified by the FE analysis to fail at the location of the tumor. For this case the FE predicted yielding load was 14% beyond the experimental yield load and 7% beyond the experimental fracture load. Although the FE analysis over-estimated the yield load, a very good yield prediction was noticed even for these highly compromised femurs.

Although the experimental yield forces were within a broad range (1700 to 10000 [N]) the predicted yield force were reasonably accurate, and for the low yield forces (less than 6000 [N]) a very good prediction was obtained. These results for a simple linear model as presented here are satisfactory for clinical usage. The predicted locations are accurate in 8 out of 14 fracture locations. Two (FFM2R and FFM6L) of the unsuccessful predictions were due to a fracture occurring in the middle of the head, close to the load application by the flat machine punch. Since FE models in the vicinity of the load did not mimic precisely the experimental setting (load was applied instead of a constant displacement on a flat surface), it is not surprising that these fracture patterns were not accurately predicted.

Analysis of the specific tumors at the fracture surfaces: FFM1, FFM4 and FFM5 showed lytic and FFM6 showed blastic tumors in their fracture surfaces, being probably a significant factor in the location of the fractures. FFM6R fractured through a significant tumor located under the greater trochanter suggesting that cortical involvement of the tumor plays an important role in the fracture site and load. When comparing to FFM6L, one may observe that metastasis in FFM6R was considerably more aggressive (this is visible in the X-rays

images and in the CT scans) significantly affecting its bearing capacity. Lytic metastases of adenocarcinoma[2] tumors were found in the two FFM1 femurs. It was found close to the fracture surface of the right FFM1 femur, and on the fracture surface in the left FFM1 femur. In the right side the tumor was much smaller. FFM1 femurs showed no reduction in their bearing capacity due to the presence of tumors, but the fracture location was affected.

One may observe that the fracture force of FFM2L is considerably lower than the other thirteen femurs. This is a consequence of extreme osteoporosis in the femur. On the other hand, the relatively large head displacement of FFM2L may indicate that the bone suffered significant plastic deformation until fracture. In these femurs the predicted yield load is 20-25% lower compared to the experiments. Although such predictions may be considered adequate for clinical applications, further investigation is planned to address such osteoporotic bones.

There are several limitations to the present study: a) A single and simplified stance position loading was applied (at three different inclination angles). More loading conditions will be applied in future studies. b) The bone tissue is inhomogeneous orthotropic or transversely isotropic and the application of inhomogeneous isotropic material properties in the FE simulations is a simplification of the reality. For a more complex state of loading, more realistic material properties would probably result in a better correlation with the in-vitro experiments. c) More sophisticated yield laws for the bone tissue, with parameters that can be measured by clinical procedures are lacking. These should be developed to include also the influence of the type of metastatic tumor on the yield law.

This study shows that the FEM method previously validated to estimate the strength of the proximal femur can also be used for estimations when metastatic lesions are present. For the method to be used as a clinical tool, further development is necessary. The time for creating the FE model and the processing time need to be automated and shortened. The technique has to be validated for additional bone anatomical sites and other clinical situations

[2]Metastases of cancer from a glandular tissue.

such as fractures. The economic cost for the service has to be delivered at a reasonable price. Additional, adapting it to a hand held communication device would make use of the method convenient to the clinician.

Conflict of Interest

None of the authors have any conflict of interest to declare that could bias the presented work.

Acknowledgements

The authors thank Mr. Ilan Gilad and Natan Levin from the Ben-Gurion University of the Negev, Israel, for their help with the experiments. The first author gratefully acknowledges the generous support of the Technical University of Munich - Institute for Advanced Study, funded by the German Excellence Initiative. This study was supported in part by grant no. 3-00000-7375 from the Chief Scientist Office of the Ministry of Health, Israel.

References

[1] A. Alho, T. Husby, and A. Hoiseth. Bone mineral content and mechanical strength. An ex-vivo study on human femora and autopsy. *Clin. Orthop.*, 227:292–297, 1988.

[2] H.H. Bayraktar, E.F. Morgan, G.L. Niebur, G.E. Morris, E.K. Wong, and M. Keaveny. Comparison of the elastic and yield properties of human femoral trabecular and cortical bone tissue. *Jour. Biomech.*, 37:27–35, 2004.

[3] R. E. Coleman. Clinical features of metastatic boned isease and risk of skeletal morbidity. *Clinical Cancer Research*, 12:6243s–6249s, 2006.

[4] T.A. Damron, H. Morgan, D. Prakash, W. Grant, J. Aronowitz, and J. Heiner. Critical evaluation of Mirels rating system for impending pathologic fractures. *Clin. Orthop. Relat. Res.*, 415:S201–S207, 2003.

[5] L. C. Derikx, J. B. van Aken, D. Janssen, A. Snyers, Y. M. van der Linden, N. Verdonschot, and E. Tanck. The assessment of the risk of fracture in femora with metastatic

lesions: Comparing case-specific finite element analyses with predictions by clinical experts. *Jour. Bone Joint Surg.*, 94-B(8):1135–1142, 2012.

[6] SI. Esses, JC. Lotz, and WC. Hayes. Biomechanical properties of the proximal femur determined in vitro by single-energy quantitative computed tomography. *Jour. Bone Mineral Res.*, 4:715–722, 1989.

[7] M.M Goodsitt. Conversion relations for quantitative ct bone mineral densities measured with solid and liquid calibration standards. *Bone. and. Mineral*, 19:145–158, 1992.

[8] B. J. Heismann, J. Leppert, and K. Stierstorfer. Density and atomic number measurements with spectral x-ray attenuation method. *J. App. Phys.*, 94:2073–2079, 2003.

[9] Muhammad Umar Jawad and Sean P. Scully. In brief: Classifications in brief: Mirels' classification: Metastatic disease in long bones and impending pathologic fracture. *Clin. Orthop. Relat. Res.*, 468(10), 2010.

[10] Alon Katz. The mechanical response of femurs fixed by metal devices. MSc thesis, Dept. of Mechanical Engineering, Ben-Gurion University of the Negev, Beer-Sheva, Israel, 2011.

[11] T. S. Keller. Predicting the compressive mechanical behavior of bone. *Jour. Biomech.*, 27:1159–1168, 1994.

[12] J.H . Keyak, M. G. Fourkas, J. M. Meagher, and H. B. Skinner. Validation of automated method of three-dimensional finite element modelling of bone. *ASME Jour. Biomech. Eng.*, 15:505–509, 1993.

[13] JH Keyak, TS Kaneko, SA Rossi, MR Pejcic, J Tehranzadeh, and HB Skinner. Predicting the strength of femoral shafts with and without metastatic lesions. *Clin. Orthop. Relat. Res.*, 439:161–170, 2005.

[14] JH Keyak, TS Kaneko, J Tehranzadeh, and HB Skinner. Predicting proximal femoral

strength using structural engineering models. *Clin. Orthop. Relat. Res.*, 437:219–228, 2005.

[15] Kenneth A. Mann, John Lee, Sarah A. Arrington, Timothy A. Damron, and Matthew J. Allen. Predicting distal femur bone strength in a murine model of tumor osteolysis. *Clin. Orthop. Relat. Res.*, 466(6):1271–1278, 2008.

[16] Javad Hazrati Marangalou, Keita Ito, and Bert van Rietbergen. A new approach to determine the accuracy of morphology-elasticity relationships in continuum FE analyses of human proximal femur. *Jour. Biomech.*, 45(16):2884–2892, 2012.

[17] Mindways Software, 282 Second St., San Francisco, CA 94105. *CT Calibration Phantom*, 2002.

[18] H. Mirels. Metastatic disease in long bones. a proposed scoring system for diagnosing impending pathologic fractures. *Clin. Orthop. Relat. Res.*, 249:256–264, 1989.

[19] John A. Rennick, Ara Nazarian, Vahid Entezari, James Kimbaris, Alan Tseng, Aidin Masoudi, Hamid Nayeb-Hashemi, Ashkan Vaziri, and Brian D. Snyder. Finite element analysis and computed tomography based structural rigidity analysis of rat tibia with simulated lytic defects. *Jour. Biomech.*, 46(15):2701 – 2709, 2013.

[20] E. Schileo, E. DallAra, F. Taddei, A. Malandrino, T. Schotkamp, M. Baleani, and M. Viceconti. An accurate estimation of bone density improves the accuracy of subject-specific finite element models. *Jour. Biomech.*, 41:2483–2491, 2008.

[21] Brian D. Snyder, Marsha A. Cordio, Ara Nazarian, S. Daniel Kwak, David J. Chang, Vahid Entezari, David Zurakowski, and Leroy M. Parker. Noninvasive prediction of fracture risk in patients with metastatic cancer to the spine. *Clin. Cancer Research*, 15(24):7676–7683, 2009.

[22] Sander Spruijt, Jacqueline C Van Der Linden, P D Sander Dijkstra, Theo Wiggers, Mathijs Oudkerk, Chris J Snijders, Fred Van Keulen, Jan A N Verhaar, Harrie Weinans,

and Bart A Swierstra. Prediction of torsional failure in 22 cadaver femora with and without simulated subtrochanteric metastatic defects: A CT scan-based finite element analysis. *Acta Orthopaedica*, 77(3):474–481, 2006.

[23] Esther Tanck, Jantien B. van Aken, Yvette M. van der Linden, H.W. Bart Schreuder, Marcin Binkowski, Henk Huizenga, and Nico Verdonschot. Pathological fracture prediction in patients with metastatic lesions can be improved with quantitative computed tomography based computer models. *Bone*, 45(4):777 – 783, 2009.

[24] N. Trabelsi and Z. Yosibash. Patient-specific FE analyses of the proximal femur with orthotropic material properties validated by experiments. *ASME Jour. Biomech. Eng.*, 155:061001–1 – 061001–11, 2011.

[25] N. Trabelsi, Z. Yosibash, and C. Milgrom. Validation of subject-specific automated p-FE analysis of the proximal femur. *Jour. Biomech.*, 42:234–241, 2009.

[26] N. Trabelsi, Z. Yosibash, C. Wutte, R. Augat, and S. Eberle. Patient-specific finite element analysis of the human femur - a double-blinded biomechanical validation. *Jour. Biomech.*, 44:1666 – 1672, 2011.

[27] Z. Yosibash, R. Padan, L. Joscowicz, and C. Milgrom. A CT-based high-order finite element analysis of the human proximal femur compared to in-vitro experiments. *ASME Jour. Biomech. Eng.*, 129(3):297–309, 2007.

[28] Z. Yosibash, R. Plitman Mayo, and C. Milgrom. Atypical viscous fracture of human femurs. *Advances in Biomech. & Appl.*, 1(2):77–83, 2014.

[29] Z. Yosibash, D. Tal, and N. Trabelsi. Predicting the yield of the proximal femur using high order finite element analysis with inhomogeneous orthotropic material properties. *Philosophycal Transaction of the Royal Society: A*, 368:2707–2723, 2010.

[30] Z. Yosibash, N. Trabelsi, and C. Hellmich. Subject-specific p-FE analysis of the proximal femur utilizing micromechanics based material properties. *Int. Jour. Multiscale Computational Engineering*, 6(5):483–498, 2008.

[31] Z. Yosibash, N. Trabelsi, and C. Milgrom. Reliable simulations of the human proximal femur by high-order finite element analysis validated by experimental observations. *Jour. Biomech.*, 40:3688–3699, 2007.